ACS Sustainable Chemistry & Engineering

Research Article

pubs.acs.org/journal/ascecg

Facile Fabrication of S-TiO_2/β-SiC Nanocomposite Photocatalyst for Hydrogen Evolution under Visible Light Irradiation

Gopa Mishra,[†,‡] K. M. Parida,*[,†,§] and S. K. Singh[†,‡]

[†]Academy of Scientific and Innovative Research (AcSIR), Council of Scientific and Industrial Research, Anusandhan Bhawan, 2 Rafi Marg, New Delhi 110 001, India

[‡]Advanced Materials Technology Department, CSIR-Institute of Minerals and Materials Technology, Bhubaneswar, 751013 Odisha, India

[§]Centre for Nano Science and Nano-Technology, ITER, Siksha 'O'Anusandhan University, Bhubaneswar, 751030 Odisha, India

ABSTRACT: A series of sulfate modified TiO_2/β-SiC nanocomposite photocatalysts has been fabricated by sol–gel and wetness impregnation method by varying amount (5–20 wt %) of sulfate contents. The photocatalysts has been characterized by X-ray diffraction (XRD), Fourier transform infrared spectroscopy (FTIR), UV–visible diffuse-reflectance spectroscopy (UV–vis DRS), Brunauer–Emmett–Teller (BET) surface area, high resolution-transmission electron microscopy (HR-TEM), X-ray photoelectron spectroscopy (XPS), photoelectrochemical (PEC) measurement and photoluminescence (PL) florescent spectra study. The finding confirms that type (II) heterojunction exists between the crystal lattice of β-SiC and TiO_2; alternatively, sulfate (S^{6+}) is bidentately coordinated on the surface of TiO_2. The existence of sulfate maintains the morphology as well as enhances the surface area, decreases the crystallite size, shifts the optical absorption toward the red end, enhances the generation of OH radical, acts as cocatalyst, and facilitates the photogenerated charge carriers. The photocatalytic activity of the synthesized catalysts has been evaluated toward hydrogen energy production in the presence of visible light. The excellent photocatalytic activity (1254 μmol in 3 h) for 15 wt % S doped TiO_2/β-SiC has been attributed to the synergistic interaction of ternary species, and establishment of heterojunction, which decreases the charge recombination rate, makes easy channelization of electron for effective surface charge transfer, and enhances the photocatalytic properties of the catalyst.

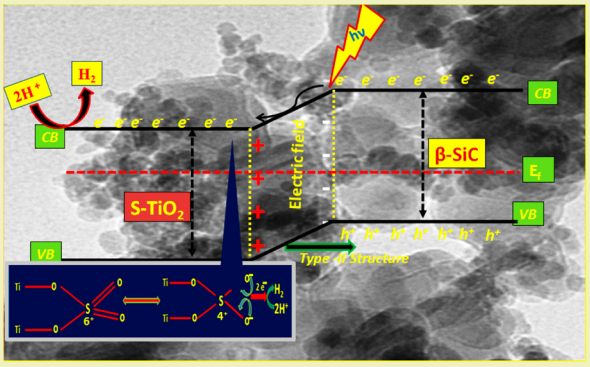

KEYWORDS: *Heterojunction, S doped TiO_2/β-SiC, visible light-harvesting, H_2 evolution*

INTRODUCTION

The search for suitable semiconductor photocatalysts for the production of hydrogen gas by splitting water using solar energy is one of the noble missions of the scientific community.[1] Since Fujishima and Honda reported in 1972 the photocatalytic activity of TiO_2 in generating hydrogen from water, photocatalytic water splitting (PWS) has been explored intensively.[2] Since then, much attention has been paid to the development of the oxide based photocatalyst.[3−5] TiO_2 has photocatalytic activity itself and is an ideal substrate for composite photocatalyst, hence, it has been intensively investigated in PWS reactions. However, the photocatalytic activity of TiO_2 itself is limited, its band gap is in UV range and the electron/hole (e/h) pairs recombination rate is too fast.[6] Therefore, doping the TiO_2 with nonmetals, transitions metals,[6−8] and heterojunctions with other oxides,[9−12] increases the surface area, improves the transfer of photogenerated electrons prolonging charge carrier lifetime, and the ability of working under visible-light irradiation. Currently, the coupling of two semiconductors is making headlines in the research area due to their promising properties like improvement of photoabsorption of the UV active materials in the visible region and also suppression of the recombination rate of the charge carriers.[9,13−15] Moreover, the coupling of two different semiconductors should have proper band edge potentials, which help to transfer the charge carriers from one semiconductor to the other. This favors the separation of photoinduced electrons and holes and thus improves the photocatalytic efficiency of the materials.[13−16] Particularly, the coupling of *n*-type TiO_2 with *p*-type narrow band gap semiconductors is a good approach to improve the visible light absorption capability and photocatalytic performance of TiO_2.

β-Silicon carbide (β-SiC) is a typical narrow band gap (2.2 eV) *p*-type nonmetallic semiconductor prominently known for its excellent physical and chemical properties such as low specific weight, insoluble in water, and chemical inertness, which are essential ingredients for heterogeneous catalytic

Received: September 3, 2014
Revised: November 5, 2014
Published: December 23, 2014

DOI: 10.1021/sc500570k
ACS Sustainable Chem. Eng. 2015, 3, 245−253

reaction. Apart from that, the metal support stability (MSS) of SiC is higher and metal support interaction (MSI) is lower in comparison to any other catalytic materials.[17−21] Gao et al. reported that SiC absorbs visible light and splits water to form hydrogen but with very low efficiency (24.9 mL g^{-1} h^{-1}).[19] The current research has focused on the combination of ternary species to enhances the catalytic activity and achieve higher efficiency.[20−22] It has been well reported that incorporation of sulfur plays a potential role in modifying the electronic structure of TiO_2 in the composite interface and enhances light absorption property.[23−25] The synthetic condition and precursors used in the reaction process have important roles for the different oxidation states of sulfur (S^{2-}, S^{4+}, and S^{6+}) in TiO_2.[23−25] Thus, modifying heterocompounds by adding sulfur is one of the most important ways to explore novel photocatalysts. In this connection, various researchers have synthesized sulfur modified nanocomposites such as S-ZnO/TiO_2, N, S-codoped TiO_2, and V_2O_5/N,S-TiO_2 for visible light active photocatalytic reaction.[24,25,6] However, there has been no report on the synthesis of a S modified SiC/TiO_2 nanocomposite and its catalytic activity study toward photocatalytic water splitting reaction. In the present work, sulfur plays a cocatalyst role in composite interface to extend the light absorption to visible range and is nonpoisonous to the environment.

In this contribution, a series of S-TiO_2/β-SiC nanocomposites with varying amounts of sulfate concentration (5−20 wt %) has been synthesized by sol−gel and wetness impregnation method. The characterization of synthesized catalysts was carried out by various physiochemical techniques. The photocatalytic performance of S-TiO_2/β-SiC nanocomposites in comparison with neat TiO_2/β-SiC toward hydrogen evolution by water splitting reaction in the presence of visible light has been carried out. Among all, 15 wt % S-TiO_2/β-SiC catalyst shows highest photocatalytic performance (418 μmol h^{-1} hydrogen gas). The impact of S concentration over the crystal structure, morphology, and optical properties of the synthesized catalyst has been studied and discussed in details.

EXPERIMENTAL SECTION

Synthesis of β-SiC/TiO_2 Nanocomposites. The heterojunction based β-SiC/TiO_2 nanocomposite was synthesized by a sol−gel process at room temperature by the hydrolysis of titanium(IV) isopropoxide (Ti $(O^iPr)_4$) (97% purity, Sigma-Aldrich) in the presence of β-SiC powder (50 nm, SRL 98%). An requisite amount of β-SiC has been dispersed in 30 mL of dry ethanol at room temperature followed by sonication for 30 min to break the agglomerated particles. Then a required amount of pure Ti $(O^iPr)_4$ was added dropwise to the suspension and stirred for another 30 min. Hydrolysis and condensation reactions of Ti $(O^iPr)_4$ were initiated through the addition of acetic acid (AA), followed by distilled water. The mixer was finally stirred in air at room temperature, resulting in a dry powder after total evaporation of the solvent. The dry powder was ground in a mortar to break the agglomeration. In this way, the TiO_2/β-SiC catalyst was prepared.

Synthesis of S-TiO_2/β-SiC Nanocomposites. A series of S-TiO_2/β-SiC heterojunction based nanocomposites was synthesized by a wetness impregnation method at room temperature by varying the concentration of sulfuric acid (H_2SO_4). A requisite amount of TiO_2/β-SiC powder was dispersed in 30 mL of distilled water and continuously stirred by a glass rod. A required amount of pure sulfuric acid (H_2SO_4) was added dropwise to the suspension (pH of the solution during the impregnation method lies in the range 3.5−4.4) and stirred for another 30 min. The mixture was stirred in air at room temperature, resulting in a dry powder after total evaporation of the solvent. The dry powder was ground in a mortar to break the agglomeration. The resulting fine powder was calcined at 450 °C for 2 h in air atmosphere at heating rate of 5 °C per minute to allow combustion of the remaining organic molecules and crystallization of the catalysts. In this way, different compositions (5, 10, 15, and 20 wt %) of S-TiO_2/β-SiC catalysts were prepared.

Material Characterization. The structure and phase identification of the prepared samples were performed by X-ray powder diffraction (XRD) technique by Philips PANalytical PW 3040/60 instrument using Cu Kα radiation 1.5405 Å within the 2θ range from 10 to 80°. The bonding and structural information on all the prepared catalysts were recorded using Fourier transform infrared spectroscopy (FTIR) by Bruker-Alpha (ECO-ATR) within the range of 500−4000 cm^{-1}. Self-supporting pellets were prepared with KBr and catalysts applying 50 kg/cm^2 pressure. These pellets were further used for recording FTIR spectra. Optical absorbance of prepared catalysts were measured by UV−visible diffuse-reflectance spectroscopy (UV−vis DRS), Varian Cary 100 spectrophotometer (model EL 96043181) equipped with a diffuse reflectance accessory in the region 200−800 nm. The spectra were recorded using boric acid as the reflectance standard. The Brunauer−Emmett−Teller (BET) surface areas of all the prepared samples were determined by N_2 adsorption−desorption studies at liquid nitrogen temperature (−197 °C) in an automated surface area and porosity analyzer (ASAP2020, Micromeritics, USA). The shape, size and composition of the prepared catalysts were determined by High resolution-transmission electron microscope (HR-TEM) equipped with energy dispersive X-ray (EDS) spectroscopy using a Twin FEI, Tecnai^2 20 instrument operated at 200 kV. The electronic states of Ti, O, Si, and C, have been examined by X-ray photoelectron spectroscopy ((XPS), Kratos Axis 165 with a dual-anode (Mg and Al) apparatus) using a Mg Kα source. All the binding energy values were calibrated by using the contaminant carbon (C 1s = 284.4 eV) as a reference. Charge neutralization of 2 eV was used to balance the charge of the sample. Binding energy values of the samples were reproducible within ±0.1 eV. The photoelectrochemical measurement (FE-SEM) was performed by potentiostat, (Versastat 3, Princeton Applied Research) using 300 W Xe lamps. For photoelectrochemical measurement, the electrodes were prepared by electrophoretic deposition in an acetone solution (30 mL) containing photocatalyst powder (30 mg) and iodine (30 mg). Two parallel FTO (fluorine doped tin oxide) electrodes were immersed in the solution with a 10−15 mm separation, and a 50 V bias was applied between the two for three min for potential control. The coated area was fixed at 1 × 3 cm and then dried. The photoelectrochemical measurement was performed using a conventional Pyrex electrochemical cell consisting of a prepared electrode, a platinum wire as a counter electrode (1 mm in diameter, 15 mm in length), and a Ag/AgCl reference electrode. The cell was filled with an aqueous solution of 0.1 M Na_2SO_4, and the pH of the solution was kept fixed to 6. The electrolyte was saturated with nitrogen prior to electrochemical measurements, and the potential of the electrode was controlled by a potentiostat (Versastat 3, Princeton Applied Research) with 300 W Xe lamps. Notably, the FTO did not show photoresponse in the solution. For $OH^•$ radical detection, the liquid PL (fluorescence spectrum) characterization was carried by LS-55 fluorescence spectrophotometer. The experiment was carried out in the presence of solar light by taking 0.02 g L^{-1} of each catalyst with 5× 10^{-4} M terephthalic acid (TPA) with a concentration of 2 × 10^{-3} M NaOH in five different tightly fitted conical flasks. The reaction solution of each individual catalyst was thoroughly centrifuged and collected in a 5 mL quartz cuvette with an excitation wavelength of 315 nm.

Photocatalytic Hydrogen Production. The catalytic activity and deactivation were studied in a batch reactor. About 0.05 g of catalyst was suspended in 50 mL of an aqueous solution containing 10 vol % of methanol solution. The solution was stirred with a magnetic stirrer. Prior to irradiation, the reaction mixture was purged with nitrogen gas for removing dissolved gases. A 125 W medium pressure Hg visible lamp was used as light source and 1 M $NaNO_2$ solution as UV filter. The evolved gas was collected by water displacement technique and was analyzed on GC-17A (Shimadzu) using a 5 Å molecular sieve

DOI: 10.1021/sc500570k
ACS Sustainable Chem. Eng. 2015, 3, 245−253

column and a thermal conductivity detector (TCD). A comparison of the retention time of the only peak that appeared on the chromatogram with standard confirmed that the gas was only hydrogen.

RESULTS AND DISCUSSION

XRD Study. The X-ray diffraction patterns of pure TiO_2/β-SiC nanocomposites along with varying amount (5−20 wt %) of S modified TiO_2/β-SiC nanocomposites are shown in Figure 1. The X-ray diffraction peaks of the pure TiO_2/β-SiC nanocomposite in Figure 1a indicate the presence of cubic β-SiC phase with lattice planes (111), (200), (220), (311), (222), and (400) (JCPDS file No. # 02-1050) along with tetragonal anatase TiO_2 phase with lattice planes (101), (200), (211), (JCPDS file No. # 21-1272). The intensity of β-SiC and TiO_2 diffraction peaks become weaker upon increasing the S concentration over TiO_2/β-SiC nanocomposites from 5 to 20 wt % (Figure 1b−e). In addition, the main diffraction peaks of TiO_2 and β-SiC in S-TiO_2/β-SiC nanocomposites become broaden and gradually shifted to lower angle region compared to pure TiO_2/β-SiC nanocomposite (inserted graph in Figure. 1). The crystallite sizes of all the synthesized samples are determined by employing Scherer's formula ($D = K\lambda/\beta\cos\theta$), where λ is the wavelength of the X-ray (Cu Kα), β is the full width at half-maximum of the diffraction peak, K is a shape factor (0.89), and θ is the angle of diffraction. The average crystallite size of all the synthesized samples is listed in Table 1. The crystallite size decreases in the presence of sulfate ions, as S species could possibly interact with the TiO_2 network, and thus hinder the growth of the crystal.[26] However, 15 wt % of S species is sufficient to lower the crystallite size for this effect. Thereafter, change in sulfate concentration did not change crystallite size further. Therefore, it has been assumed that a 15 wt % of S loading is optimum condition for lowering the crystallite size of TiO_2/β-SiC nanocomposite. It might be one of the possible factors toward higher photocatalytic activity.

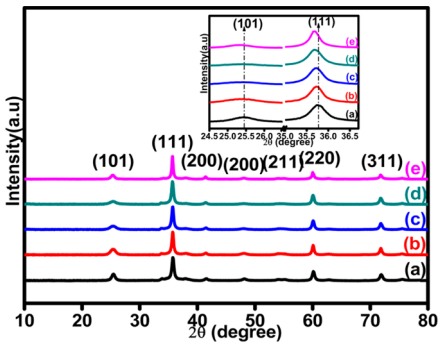

Figure 1. X-ray diffraction patterns of (a) TiO_2/β-SiC, (b) 5 wt % S-TiO_2/β-SiC, (c) 10 wt % S-TiO_2/β-SiC, (d) 15 wt % S-TiO_2/β-SiC, (e) 20 wt % S-TiO_2/β-SiC.

Table 1. Crystallite Size, BET Surface Area, Pore Size, and Pore Volume the Synthesized Catalysts

sample code	crystallite size (nm)	BET surface area (m^2/g)	pore size (Å)	pore volume (cm^3/g)
TiO_2/β-SiC	39.41	38.2	106.69	0.15
5 wt % S-TiO_2/β-SiC	14.17	41.5	113.48	0.18
10 wt % S-TiO_2/β-SiC	11.95	63.8	413.66	0.29
15 wt % S-TiO_2/β-SiC	9.87	98.2	602.46	0.47
20 wt % S-TiO_2/β-SiC	10.91	89.0	814.72	0.58

FTIR Study. The FTIR spectra of pure TiO_2/β-SiC and different (5−20) wt % of S modified TiO_2/β-SiC are shown in Figure 2. The peak corresponding to 1215 cm^{-1} is the stretching frequency of S═O, and the two small humps that arise at 1131 and 1093 cm^{-1} are the characteristic frequencies of bidentate SO_4^{2-}coordinate to Ti^{4+} (Figure 2b−e).[26−28] The peaks at 587 and 847 cm^{-1} correspond to vibrational mode of O−Ti−O bond and transverse optical mode of nano Si−C, respectively (Figure 2a−e).[29−31] The broad absorption band in the region of 3200−3600 cm^{-1} is characteristic of the OH stretching vibration of surface hydroxyl groups and the peak corresponding to 1619 cm^{-1} has been assigned to H−O−H bending of physically adsorbed water (Figure 2a−e).[32] The band corresponding to 2355 cm^{-1} is the presence of $TiOH_2$.[33] This is the interaction of adsorbed water with TiO_2. A close observation of Figure 2 suggests that after different wt % of S loading over TiO_2/β-SiC nanocomposite, the TiO_2 peaks are broaden and gradually shifted toward lower wavenumber regions. The maximum peak shifting at 15 wt % S-TiO_2/β-SiC is the result of optimization of S-doping over TiO_2/β-SiC nanocomposite and a close interaction of ternary components at the heterojunction interface which has been consistent with the observed XRD results.

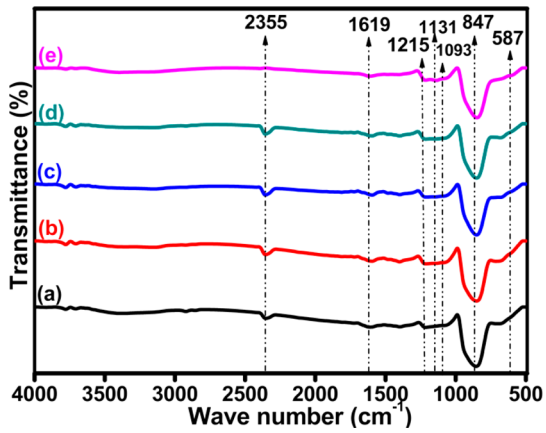

Figure 2. Fourier transform infrared spectroscopy of (a) TiO_2/β-SiC, (b) 5 wt % S-TiO_2/β-SiC, (c) 10 wt % S-TiO_2/β-SiC, (d) 15 wt % S-TiO_2/β-SiC, and (e) 20 wt % S-TiO_2/β-SiC.

DRS Study. Figure 3 depicts the UV−visible spectra of pure TiO_2/β-SiC and different (5−20) wt % of S modified TiO_2/β-SiC. TiO_2 shows an intense UV absorption band in the range 200−400 nm whereas β-SiC exhibits a wonderful absorption band extending from the UV region to the visible range, i.e., 400−543 nm, which suggests the formation of heterojunction in TiO_2/β-SiC nanocomposite (Figure 3a).[34] As shown in Figure 3, a significant red shift in the absorption edge has been noticed for S modified TiO_2/β-SiC nanocomosite in comparison to parent TiO_2/β-SiC. The maximum shifting has been observed in the 15 wt % S-TiO_2/β-SiC nanocomposite (Figure 3d), which explains the optimization of S doping on the TiO_2 surface. The remarkable red shifting of the S-TiO_2/β-SiC photocatalyst toward visible light absorbance is attributed to the coexistence of the β-SiC, TiO_2, and S species. The heterojunction of β-SiC with TiO_2 and the intermixing of S

DOI: 10.1021/sc500570k
ACS Sustainable Chem. Eng. 2015, 3, 245−253

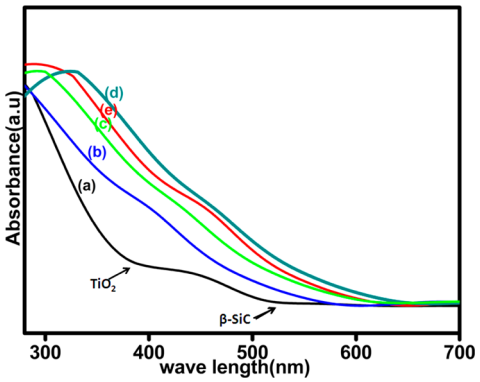

Figure 3. UV−vis diffuse reflectance spectroscopy of (a) TiO_2/β-SiC, (b) 5 wt % S-TiO_2/β-SiC, (c) 10 wt % S-TiO_2/β-SiC, (d) 15 wt % S-TiO_2/β-SiC, and (e) 20 wt % S-TiO_2/β-SiC.

3p and O 2p states of TiO_2 creates a localized state just above the valence band and subsequently narrows the energy gap.[34−36] Again, a recent study reveals that the cationic S doping creates an additional S 3p level 0.38 eV above of the valence band of TiO_2 and narrows the energy gap of the composite.[37] Hence this study suggests higher catalytic activity of S modified TiO_2/β-SiC nanocomosite in the presence of visible light.

BET Surface Area. To understand the textural properties, all the synthesized catalyst has been subjected to N_2 adsorption/desorption measurements. The result has been summarized in Table 1. The highest value has been observed in case of 15 wt % S-TiO_2/β-SiC (98.2 m^2/g). Here, the observed-enhanced specific surface area (for 15 wt % S-TiO_2/β-SiC) has been consistent with the crystallite size (calculated from XRD).[38] However, after sulfate loading, the anatase phase is well anchored by tetrahedral sulfate groups that hinders the crystallite growth as well as maintains the morphology and porosity of the composite. However, at higher wt % sulfate loading, i.e., at 20 wt % S-TiO_2/β-SiC, an irregular pore size distribution has been noticed in comparison to various S-TiO_2/β-SiC photocatalysts, which might be due to excess sulfate. Sometimes, an excess amount of sulfate deactivates the catalytic activity.[32]

HR-TEM Study. Figure 4 explains the transmission electron microscopy (TEM) and energy dispersive X-ray (EDS) spectrum of neat TiO_2/β-SiC and different (5−20) wt % of S modified TiO_2/SiC nanocomposite. The pristine TiO_2/SiC catalyst shows an irregular morphology with close interaction between cubic phase β-SiC and spherical shape TiO_2 (Figure 4a). This type of morphology has been observed in the case of a heterojunction reported in the literature.[39,40] From the figure, it has been observed that the average particle sizes of neat TiO_2/β-SiC catalyst is 10−70 nm. Further, the EDS analysis supports the coexistence of both β-SiC and TiO_2 phase in TiO_2/β-SiC nanocomposite (Figure 4a). There has been no significant S peak observed on the surface of neat TiO_2/β-SiC nanocomposite. After increasing sulfate doping, the morphology of TiO_2/β-SiC nanocomposite gradually changes, as shown in Figure 4b−e. In the case of the 15 wt % S-TiO_2/β-SiC catalyst, a snow flake shape morphology has been observed because the sulfate species seems to have been adsorbed on the surface of the TiO_2/β-SiC nanocomposite (Figure 4d). The particle size of 15 wt % S-TiO_2/β-SiC is found to be around 10 to 50 nm. EDS spectroscopy illustrates that the sample is mainly

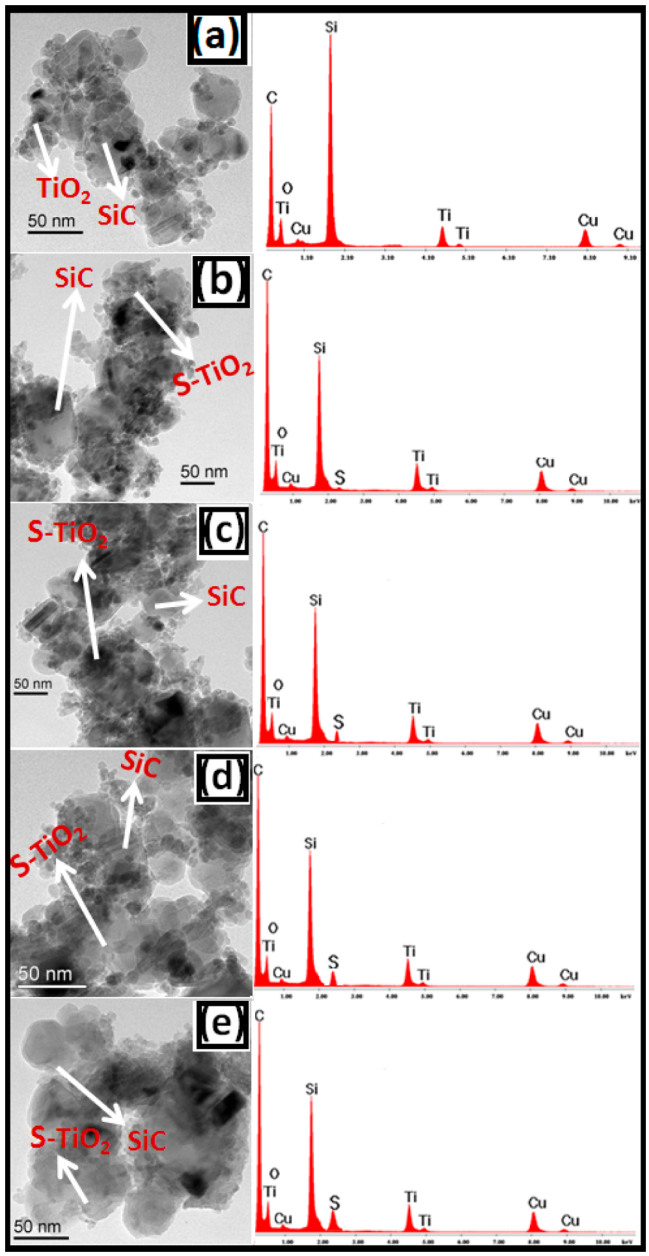

Figure 4. Transmission electron microscopy (TEM) images and energy dispersive X-ray (EDS) spectrum of (a) TiO_2/β-SiC, (b) 5 wt % S-TiO_2/β-SiC, (c) 10 wt % S-TiO_2/β-SiC, (d) 15 wt % S-TiO_2/β-SiC, and (e) 20 wt % S-TiO_2/β-SiC.

composed of Ti, O, Si, C, and S elements (Figure 4d).[37] Figure 5 describes the (a) HR-TEM image and (b) selected area electron diffraction (SAED) pattern of the 15 wt % S-TiO_2/β-SiC nanocomposite. From the HR-TEM micrograph, it has been clearly observed that well-defined lattice fringe separation with d = 0.35 nm of the (101) plane corresponds to anatase phase of TiO_2 crystal whereas the fringe separation with d = 0.25 nm of (111) planes corresponds to cubic phase of SiC crystals. The SAED image shows that both β-SiC (d values = 0.15 and 0.13 nm) and S modified TiO_2 particles (0.23 nm) are polycrystalline in nature. The existence of intimate contact between β-SiC, TiO_2 and S indicates the formation of electron-transfer center which leads the key role for higher photo-catalytic activity.

DOI: 10.1021/sc500570k
ACS Sustainable Chem. Eng. 2015, 3, 245−253

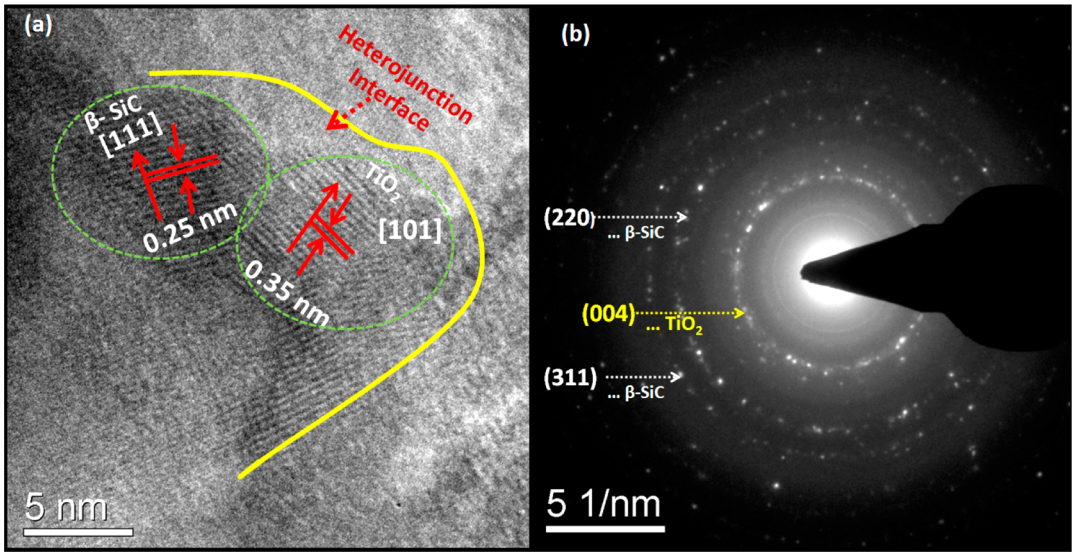

Figure 5. (a) High-resolution transmission electron microscopy (HR-TEM) image and (b) selected area electron diffraction (SAED) patterns of 15 wt % S-TiO_2/β-SiC nanocomposite catalyst.

XPS Study. Figure 6 illustrates the XPS spectra of TiO_2/β-SiC and 15 wt % S-TiO_2/β-SiC nanocomposite including C 1s, Si 2p, O 1s, Ti 2p, and S 2p core levels. The C 1s peak of pure TiO_2/β-SiC in Figure 6a shows two peaks at 282.3 and 284.5 eV assigned to C−Si and C−C bonds in SiC lattice, respectively.[34,41,42] The Si 2p peak of neat TiO_2/β-SiC in Figure 6(b) shows a strong peak at 100.4 eV along with a small peak at 102.6 eV assigned to Si−C bond and Si−O bonds, respectively.[41] The O 1s peak of TiO_2/β-SiC shows two peaks with binding energies of 530.6 and 532.3 eV Figure 6c, assigned to bulk O^{2-} from TiO_2 and Si−O/hydroxyl group (OH) usually adsorbed on the surface of the catalyst, respectively.[43,44,41] The Ti 2p peak of pure TiO_2/β-SiC (Figure 6d), shows the characteristic doublet at 458.1 eV (Ti $2p_{3/2}$) and 463.9 eV (Ti $2p_{1/2}$) with a peak separation of 5.7 eV, assigned to the Ti^{4+} state of TiO_2.[45,46] However, after S doping C 1s, Si 2p, O 1s, and Ti 2p peaks of 15 wt % S-TiO_2/β-SiC nanocomposite are shifting toward lower binding energy region, as shown in Figure 6a−d. The peak shifting suggests the strong interaction between the bridging bidentate structures of sulfate with Ti, which withdraws electron from the Ti.[47] Figure 6e shows the S 2p core level peak of 15 wt % S-TiO_2/β-SiC nanocomposite around 168.5 eV; however, this is absent in the case of the raw TiO_2/β-SiC nanocomposite. The observed peak has been attributed to the incorporation of SO_4^{2-} to the TiO_2 network and exists as S^{6+}.[48] As the sulfate group cannot enter into the TiO_2 lattice, it has been chemisorbed into the system and forms a bidentate linkage with Ti^{4+} ions.[48] This is consistent with the obtained FTIR peaks.

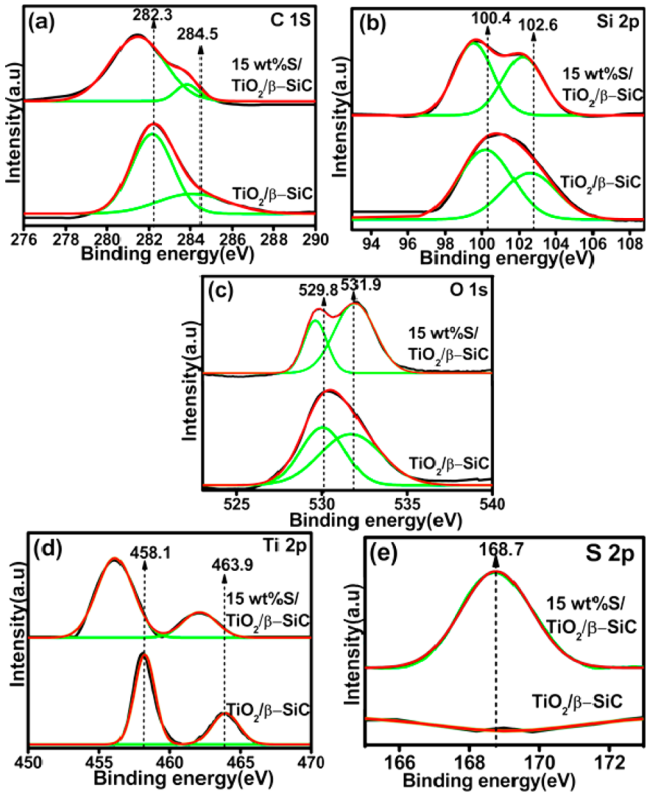

Figure 6. XPS spectra of TiO_2/β-SiC and 15 wt % S-TiO_2/β-SiC: (a) C 1s, (b) Si 2p, (c) O 1s, (d) Ti 2p, (d) S 2p.

PEC Study. Figure 7 shows the photocurrent spectra of (a) TiO_2/β-SiC and (b) 15 wt % S-TiO_2/β-SiC nanocomposite at pH 6 vs Ag/AgCl electrode in 0.1 M Na_2SO_4 solution. From the figure, it has been observed that the 15 wt % S-TiO_2/β-SiC nanocomposite photocatalyst generates more of photocurrent with applied potential under visible light conditions in comparison to raw TiO_2/β-SiC. This may be due to presence of sulfur, which exhibits the absorption of visible light because the p states of S contribute to band gap narrowing by mixing with the O 2p states of TiO_2.[35,36] In the present investigation, after S doping, both β-SiC and TiO_2 have more negative conduction band edge potentials than the hydrogen evolution potential. The relative conduction band edge potential of β-SiC and TiO_2 are suitable for water reduction reactions.

Photocatalytic Activity. *Photocatalytic Hydrogen Production.* To evaluate the catalytic activities of all the synthesized samples (neat TiO_2/β-SiC and different (5−20) wt % of S modified TiO_2/SiC nanocomposite), the photocatalytic hydrogen evolution has been carried out under visible light irradiation ($\lambda \geq 400$ nm). The reaction has been

DOI: 10.1021/sc500570k
ACS Sustainable Chem. Eng. 2015, 3, 245−253

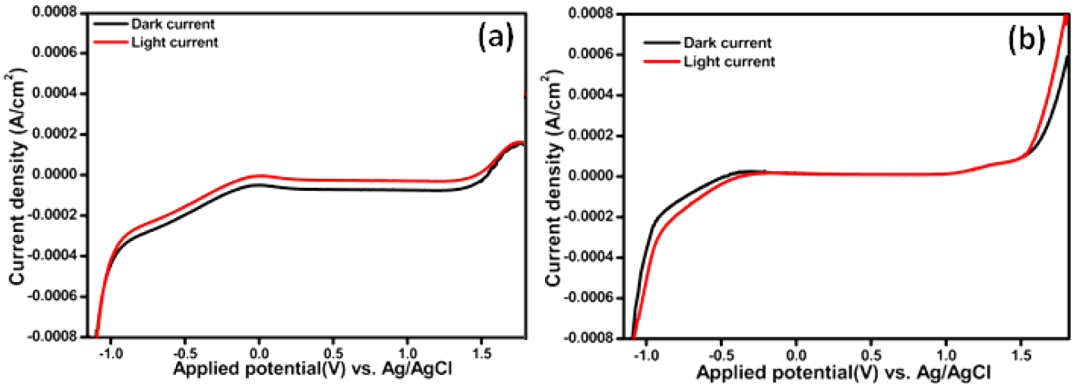

Figure 7. Current–potential curves of (a) TiO_2/β-SiC and (b) 15 wt % S-TiO_2/β-SiC nanocomposite photocatalyst.

performed by taking 0.05 g of catalyst in 50 mL of 10 vol % methanol solution. Before the photocatalytic reaction process, a blank experiment has been carried out without the catalyst as well as with the catalyst in the absence of light. Both experiments confirm no hydrogen evolution occurs. Figure 8

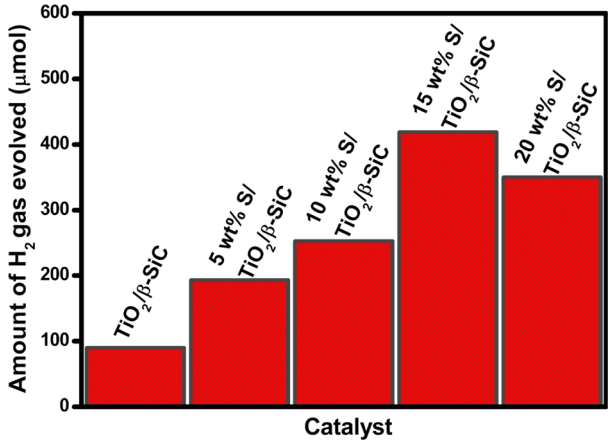

Figure 8. Photocatalytic hydrogen generation over TiO_2/β-SiC and different wt % of S-TiO_2/β-SiC nanocomposites under under visible light irradiation ($\lambda \geq 400$ nm).

shows the hydrogen production over neat TiO_2/β-SiC and different wt % of S doped TiO_2/β-SiC nanocomposites. All these photocatalysts are active toward H_2 evolution under visible light irradiation. In the company of all prepared photocatalysts, the 15 wt % S modified TiO_2/β-SiC nanocomposite shows the best activity toward hydrogen production under visible light irradiation, i.e., 418 μmol h^{-1}. It has been confirmed from the experiment that small amounts of sulfate incorporation (up to 15 wt %) steadily enhance the photocatalytic activity. However, further sulfate incorporation makes the catalyst body poison which hinders the photocatalytic reaction. To confirm the stability of the 15 wt % S modified TiO_2/β-SiC nanocomposite photocatalyst, a recyclability test was performed, and the results are shown in Figure 9. The photocatalyst could evolve 1254 μmol of H_2 in the initial 3 h of photocatalytic reaction. In every 3 h of reaction, the reactor was evacuated and the photocatalytic experiments were repeated. The activity has been found to be almost the same in all four successive runs.

The enhancement of the photocatalytic activity over the 15 wt % S modified TiO_2/β-SiC nanocomposite can be attributed to several factors discussed as follows. It is well-known that

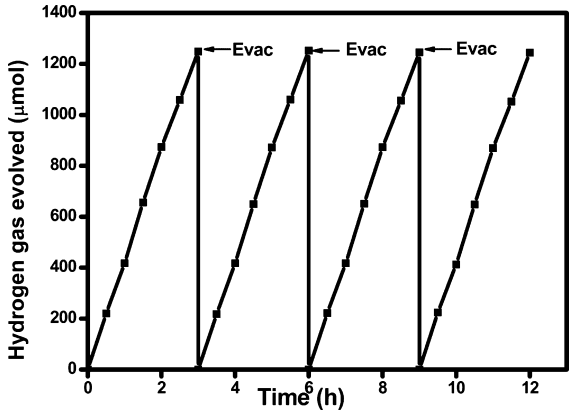

Figure 9. Reusability study over 15 wt % S-TiO_2/β-SiC nanocomposite photocatalyst for H_2 evolution under visible light irradiation.

heterogeneous photocatalysis is a surface-based phenomenon; thus, a larger specific surface area can provide more adsorption sites and photocatalytic reaction centers.[49] In the present case, in comparison to all the synthesized catalyst 15 wt % S modified TiO_2/β-SiC shows highest specific surface area for higher catalytic activity. From the photocurrent spectra, we found that β-SiC is a *p*-type semiconductor and TiO_2 is an *n*-type semiconductor.[34] As soon as *p*-type β-SiC combines with *n*-type TiO_2, a type-II band structure (*p*-*n* junction) is formed between them and the charge carriers diffuse in the opposite direction to form an electric field at the heterojunction interface.[50,51] According to the type-II band structure, the conduction band (CB) and valence band (VB) of β-SiC lie above the conduction band (CB) and valence band (VB) of TiO_2. When visible light is supplied to the β-SiC/TiO_2 nanocomposite, β-SiC absorbs the photon of energy greater than the band gap energy, which excites the electrons in the VB to the CB and leaves the holes in the VB of β-SiC. The electrons in the conduction band of *p*-type β-SiC are then transferred to *n*-type TiO_2 and holes remain in the valence band of β-SiC. The migration of photogenerated charge carriers can be promoted by the inner electric field established at the heterojunction interfaces. Consequently, the photogenerated electron–hole pairs will be effectively separated due to the formation of junction between *p*-type β-SiC and *n*-type TiO_2 interface, resulting a reduced electron hole recombination.[50,52] The separated electron and holes are then free to initiate the water splitting reaction on the surface of the photocatalyst.[52]

DOI: 10.1021/sc500570k
ACS Sustainable Chem. Eng. 2015, 3, 245–253

Scheme 1. Mechanism of Photocatalytic Hydrogen Production over 15 wt % S-TiO_2/β-SiC Photocatalyst

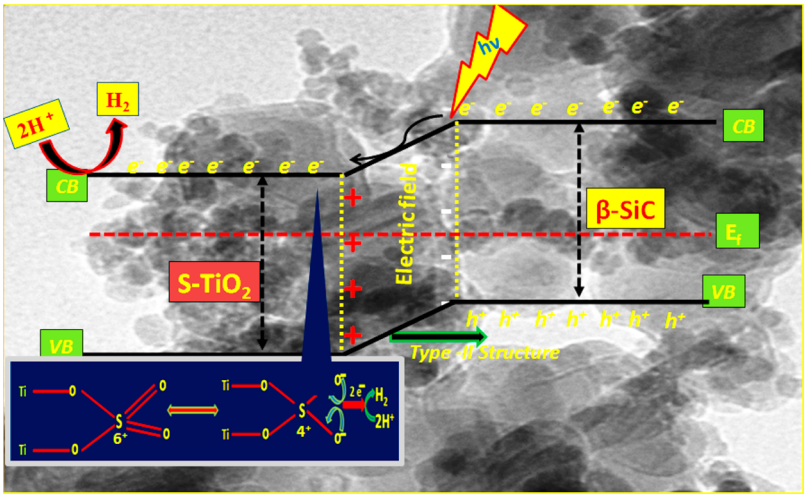

Another most crucial factor for enhanced photocatalytic activity is the incorporation of sulfate to the TiO_2 network, which forms a trap state. In the photocatalytic reaction process, coupling of the smaller crystallite size and high crystallinity anatase phase enhances the easy diffusion of photogenerated charge carriers toward the surface and rapidly reacts with the adsorbed reactant, which can contribute to improved photocatalytic activity. Moreover, the presence of surface acid sites may trap the photogenerated electrons. This phenomenon effectively separates the photogenerated charge carriers and prevents the recombination process, which leads to enhancing the water reduction reaction.[53] Considering the observed findings, a possible visible light mechanism over the 15 wt % S modified TiO_2/β-SiC photocatalyst has been proposed and is shown in Scheme 1. The formation of type-II heterostructure between TiO_2 and β-SiC successfully reduces the band gap by forming an electric field and helps to shift the optical absorbance toward the visible region. Moreover, the existence of sulfate maintains the morphology as well as enhances the surface area, decreases the crystallite size, shifts the optical absorption toward the red end, and acts as a cocatalyst.[54] Here, sulfate exists as Ti−O−S in the form of S^{6+} and acts as the center to capture photoinduced electrons. The surface adsorbed S^{6+} cation trapped photoexcited electrons from the conduction band and easily reduces the system from S^{6+} to S^{4+}.[55,27] The transferred electrons facilitate the water reduction process for the formation of H_2 gas on its surface.

Scheme 1 illustrates the mechanism of visible light absorption, easy channelization, and separation of photogenerated charge carriers through the heterojunction interface and the presence of adsorbed sulfate species on the composite surface enhance the photocatalytic activity toward H_2 evolution. So, overall, synergetic combination of small crystallite size, high specific surface area, narrow band gap, type-II heterojunction, enhanced light harvesting ability, and easy channelization of photogenerated charge carriers makes the system more potential toward visible light water-splitting.

Photoluminescence (PL) Study. Figure 10 explains the fluorescence emission spectra of all the prepared photocatalysts after 1 h of irradiation. The intensity of the fluorescent peak at around 425 nm is directly proportional to the amount of $OH^•$ radicals produced in water.[56] Greater the formation of $OH^•$ radicals, higher the separation rate of e^- and h^+ pairs in the photocatalysts. Therefore, the photocatalytic activity has positive correlation to the formation of radicals.[57,58] The formation of hydroxyl radicals over all the prepared photocatalysts followed the order: 15 wt % S-TiO_2/β-SiC > 20 wt % S-TiO_2/β-SiC > 10 wt % S-TiO_2/β-SiC > 5 wt % S-TiO_2/β-SiC > raw TiO_2/β-SiC, which agrees well with photocatalytic activity. The presence of optimum amount of sulfate ions on the surface of the 15 wt % S-TiO_2/β-SiC catalyst favors migration of photoinduced electrons, thus improving the electron−hole separation phenomenon and exhibiting higher photocatalytic activity.

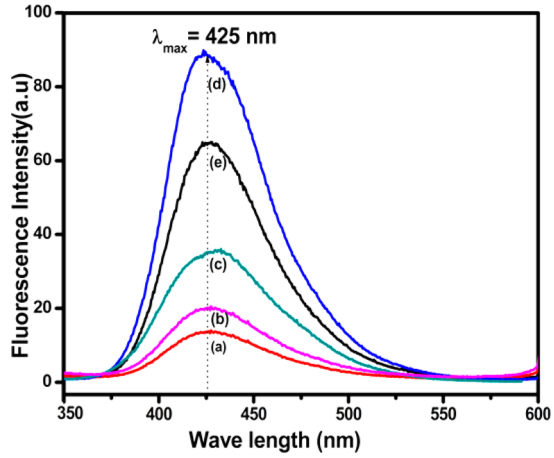

Figure 10. Fluorescence emission spectrum of (a) TiO_2/β-SiC, (b) 5 wt % S-TiO_2/β-SiC, (c) 10 wt % S-TiO_2/β-SiC, (d) 15 wt % S-TiO_2/β-SiC, and (e) 20 wt % S-TiO_2/β-SiC.

CONCLUSIONS

A series of sulfate modified TiO_2/β-SiC photocatalysts has been successfully fabricated by using a sol−gel and wetness impregnation method. The effect of sulfate modification and formation of *p*-type β-SiC/*n*-type TiO_2 heterojunction has been confirmed by XRD, XPS, and HRTEM with SAED results. The surface morphology, synergetic interaction between S, TiO_2, and β-SiC in S modified TiO_2/β-SiC nanocomposite has been well explained by FTIR, XPS, and TEM with EDS study. The effect of sulfate loading over TiO_2/β-SiC for band gap narrowing has been well supported by UV−vis DRS. The

DOI: 10.1021/sc500570k
ACS Sustainable Chem. Eng. 2015, 3, 245−253

separation of the photogenerated charge carriers, which leads to enhanced photocatalytic activities, is supported by fluorescence spectra and photocurrent measurement. Moreover, the existence of a heterojunction and the substitutional S incorporation have played pivotal roles toward visible light absorption and enhances the light-harvesting ability as well as channelize the photogenerated charge carriers and effectively suppressing the electron−hole recombination. Among all the catalysts, 15 wt % S-TiO_2/β-SiC shows the highest result of (1254 μmol in 3 h) of H_2 gas evolution in the presence of visible light. This study supports that S modified TiO_2/β-SiC composite is a promising visible light-active photocatalyst that may have potential for effective utilization of visible light.

AUTHOR INFORMATION

Corresponding Author

*K. M. Parida. E-mail: kulamaniparida@soauniversity.ac.in, paridakulamani@yahoo.com. Tel.: +91-674-2351777.

Notes

The authors declare no competing financial interest.

ACKNOWLEDGMENTS

The authors are grateful to Mr Ajit Dash, for his stable help in TEM analysis. One of the authors, Gopa Mishra, is thankful to CSIR-New Delhi for the award of SRF.

REFERENCES

(1) Rajeshwar, K.; Tacconi, N. R. Solution combustion synthesis of oxide semiconductors for solar energy conversion and environmental remediation. *Chem. Soc. Rev.* **2009**, *38*, 1984−98.

(2) Fujishima, A.; Honda, K. Electrochemical photolysis of water at a semiconductor electrode. *Nature.* **1972**, *238*, 37−8.

(3) Yang, M. Q.; Zhang, N.; Pagliaro, M.; Xu, Y. J. Artificial photosynthesis over graphene-semiconductor composites. Are we getting better? *Chem. Soc. Rev.* **2014**, *43*, 8240−8254.

(4) Zhang, N.; Ciriminna, R.; Pagliaro, M.; Xu, Y. J. Nanochemistry-derived Bi_2WO_6 nanostructures: Towards production of sustainable chemicals and fuels induced by visible light. *Chem. Soc. Rev.* **2014**, *43*, 5276−5287.

(5) Zhang, N.; Zhang, Y.; Xu, Y. J. Recent progress on graphene-based photocatalysts: Current status and future perspectives. *Nanoscale.* **2012**, *4*, 5792−5813.

(6) Martha, S.; Das, D. P.; Biswal, N.; Parida, K. M. Facile synthesis of visible light responsive V_2O_5/N, S-TiO_2 composite photocatalyst: Enhanced hydrogen production and phenol degradation. *J. Mater. Chem.* **2012**, *22*, 10695−10703.

(7) Bai, J.; Li, J.; Liu, Y.; Zhou, B.; Cai, W. A new glass substrate photoelectrocatalytic electrode for efficient visible-light hydrogen production: CdS sensitized TiO_2 nanotube arrays. *Appl. Catal., B* **2010**, *95*, 408−413.

(8) Xie, Y.; Ali, G.; Yoo, S. H.; Cho, S. O. Sonication-assisted synthesis of CdS quantum-dot-sensitized TiO_2 nanotube arrays with enhanced photoelectrochemical and photocatalytic activity. *ACS Appl. Mater. Interfaces* **2010**, *2*, 2910−2914.

(9) Bessekhouad, Y.; Robert, D.; Weber, J. V. Bi_2S_3/TiO_2 and CdS/TiO_2 heterojunctions as an available configuration for photocatalytic degradation of organic pollutant. *J. Photochem. Photobiol., A* **2004**, *163*, 569−580.

(10) Mu, J.; Chen, B.; Zhang, M.; Guo, Z.; Zhang, P.; Zhang, Z.; Sun, Y.; Shao, C.; Liu, Y. Enhancement of the visible-light photocatalytic activity of In_2O_3-TiO_2 nanofiber heteroarchitectures. *ACS Appl. Mater. Interfaces.* **2012**, *4*, 424−430.

(11) Zhang, Y.; Tang, Z. R.; Fu, X.; Xu, Y. J. TiO_2-Graphene nanocomposites for gas-phase photocatalytic degradation of volatile aromatic pollutant: Is TiO_2-Graphene Truly Different from other TiO_2-carbon composite materials? *ACS Nano* **2010**, *4*, 7303−7314.

(12) Li, W.; Cui, X.; Wang, P.; Shao, Y.; Li, D.; Teng, F. Enhanced photosensitized degradation of rhodamine B on CdS/TiO_2 nanocomposites under visible light irradiation. *Mater. Res. Bull.* **2013**, *48*, 3025−3031.

(13) Yuan, J.; Li, H.; Gao, S.; Linb, Y.; Li, H. A facile route to n-type TiO_2-nanotube/p-type boron-doped-diamond heterojunction for highly efficient photocatalysts. *Chem.Commun.* **2010**, *46*, 3119−3121.

(14) Yildirim, N.; Serin, T.; Serin, N. Investigation of a p-CuO/n-TiO_2 thin film heterojunction fabricated by the sol-gel process. *J. Optoelectron. Adv. Mater.* **2010**, *12*, 1153−1156.

(15) Han, C.; Yang, M. Q.; Weng, B.; Xu, Y. J. Improving the photocatalytic activity and anti-photocorrosion of semiconductor ZnO by coupling with versatile carbon. *Phys. Chem. Chem. Phys.* **2014**, *16*, 16891−16903.

(16) Yang, M. Q.; Xu, Y. J. Selective photoredox using graphene-based composite photocatalysts. *Phys. Chem. Chem. Phys.* **2013**, *15*, 19102−19118.

(17) Ledoux, M. J.; Huu, C. P. Silicon Carbide: A novel catalyst support for heterogeneous catalysis. *CATTECH* **2001**, *5*, 226−246.

(18) Zhou, Y.; Li, X.; Pan, X.; Bao, X. A highly active and stable Pd-TiO_2/CDC-SiC catalyst for hydrogenation of 4-carboxybenzaldehyde. *J. Mater. Chem.* **2012**, *22*, 14155−14159.

(19) Gao, Y.; Wang, Y.; Wang, Y. Photocatalytic hydrogen evolution from water on SiC under visible light irradiation. *React. Kinet. Catal. Lett.* **2007**, *91*, 13−19.

(20) Keller, V.; Garin, F. Photocatalytic behavior of a new composite ternary system: WO_3/SiC-TiO_2. Effect of the coupling of semiconductors and oxides in photocatalytic oxidation of methylethylketone in the gas phase. *Catal.Commun.* **2003**, *4*, 377−383.

(21) Zhanga, Y.; Xua, Y.; Li, T.; Wang, Y. Preparation of ternary Cr_2O_3-SiC-TiO_2 composites for the photocatalytic production of hydrogen. *Particuology* **2012**, *10*, 46−50.

(22) Rajaambal, S.; Mapa, M.; Gopinath, C. S. In1xGaxN@ZnO: A rationally designed and quantum dot integrated material for water splitting and solar harvesting applications. *Dalton Trans.* **2014**, *43*, 12546−12554.

(23) Umebayashi, T.; Yamaki, T.; Itoh, H.; Asai, K. Band gap narrowing of titanium dioxide by sulfur doping. *Appl. Phys. Lett.* **2002**, *81*, 454−456.

(24) Liao, S.; Donggen, H.; Yu, D.; Su, Y.; Yuan, G. Preparation and characterization of ZnO/TiO_2, $SO4^{2-}$/ZnO/TiO_2 photocatalyst and their photocatalysis. *J. Photochem. Photobiol., A* **2004**, *168*, 7−13.

(25) Sathish, M.; Viswanath, R. P.; Gopinath, C. S. N, S-Co-doped TiO_2 nanophotocatalyst: Synthesis, electronic structure and photocatalysis. *J. Nanosci. Nanotechnol.* **2009**, *9*, 423−432.

(26) Samantaray, S. K.; Parida, K. M. Effect of anions on the textural and catalytic activity of titania. *J. Mater. Sci.* **2003**, *38*, 1835−48.

(27) Naik, B.; Parida, K. M.; Gopinath, C. S. Facile synthesis of N- and S- incorporated nanocrystalline TiO_2 and direct solar light driven photocatalytic activity. *J. Phys. Chem. C* **2010**, *114*, 19473−19482.

(28) Rengifo-Herrera, J. A.; Pulgarin, C. Photocatalytic activity of N, S co-doped and N-doped commercial anatase TiO_2 powders towards phenol oxidation and *E. coli* inactivation under simulated solar light irradiation. *Sol. Energy* **2010**, *84*, 37−43.

(29) Suprabha, T.; Roy, H. G.; Thomas, J.; Kumar, K. P.; Methew, S. Microwave-assisted synthesis of titania nanocubes, nanospheres and nanorods for photocatalytic dye degradation. *Nanoscale Res. Lett.* **2008**, *4*, 144−152.

(30) Hilonga, A.; Kim, J. K.; Sarawade, P. B.; Kim, H. T. Rapid synthesis of homogeneous titania-silica composite with high-BET surface area. *Powder Technol.* **2010**, *199*, 284−288.

(31) Patyk, J.; Rich, R.; Wieligor, M.; Zerd, T. W. Silicon Carbide nanowires synthesis and preliminary investigations. *Acta Phys. Polym., A* **2010**, *118*, 480−482.

(32) Parida, K. M.; Sahu, N.; Biswal, N. R.; Naik, B.; Pradhan, A. C. Preparation, characterization, and photocatalytic activity of sulfate modified titania for degradation of methyl orange under visible light. *J. Colloid Interface Sci.* **2008**, *318*, 231−237.

DOI: 10.1021/sc500570k
ACS Sustainable Chem. Eng. 2015, 3, 245−253

(33) Corner, P. A.; Dobson, K. D.; James McQuillan, A. Infrared spectroscopy of the TiO_2/aqueous solution interface. *Langmuir* **1999**, *15*, 2402−2408.
(34) Mishra, G.; Parida, K. M.; Singh, S. K. Solar light driven rhodamine B degradation over highly active β-SiC-TiO_2 nanocomposite. *RSC Adv.* **2014**, *4*, 2918−12928.
(35) Umebayashi, T.; Yamaki, T.; Itoh, H.; Asai, K. Band gap narrowing of titanium dioxide by sulfur doping. *Appl. Phys. Lett.* **2002**, *81*, 454−456.
(36) Ohno, T. Preparation of visible light active S-doped TiO_2 photocatalysts and their photocatalytic activities. *Water Sci. Technol.* **2004**, *49*, 159−163.
(37) Tian, F.; Liu, C.; Zhao, W.; Wang, X.; Wang, Z.; Yu, J. C. Cationic S-doped anatase TiO_2: A DFT study. *J. Comput. Sci. Eng.* **2011**, *1*, 33−41.
(38) Khalaf, H. A. Textural properties of sulfated iron hydroxide promoted with aluminum. *Monatsh. Chem.* **2009**, *140*, 669−674.
(39) Fu, J.; Chang, B.; Tian, Y.; Xi, F.; Dong, X. Novel C_3N_4-CdS composite photocatalysts with organic−inorganic heterojunctions: *in situ* synthesis, exceptional activity, high stability and photocatalytic mechanism. *J. Mater. Chem. A* **2013**, *1*, 3083−3090.
(40) Jia, Y.; Shen, S.; Wang, D.; Wang, X.; Shi, J.; Zhang, F.; Han, H.; Li, C. Composite $Sr_2TiO_4/SrTiO_3$(La,Cr) heterojunction based photocatalyst for hydrogen production under visible light irradiation. *J. Mater. Chem. A* **2013**, *1*, 7905−7912.
(41) Binner, J.; Zhang, Y. Characterization of silicon carbide and silicon powders by XPS and zeta potential measurement. *J. Mater. Sci. Lett.* **2001**, *20*, 123−126.
(42) Mishra, G.; Behera, G. C.; Singh, S. K.; Parida, K. M. Liquid phase esterification of acetic acid over WO_3 promoted β-SiC in a solvent free system. *Dalton Trans.* **2012**, *41*, 14299−14308.
(43) Richter, J. H.; Karlsson, P. G.; Westin, G.; Blomquist, J.; Uvdal, P.; Siegbahn, H.; Sandell, A. Li Insertion in Sol-Gel Prepared Mn-Doped TiO_2 Studied by Electron Spectroscopy in Ultrahigh Vacuum. *J. Phys. Chem. C* **2007**, *111*, 3459−3466.
(44) Park, H.; Kim, H. G.; Choi, W. Y. Characterizations of highly ordered TiO_2 nanotube arrays obtained by anodic oxidation. *Trans. Electr. Electron. Mater.* **2010**, *11*, 112−115.
(45) Chai, B.; Peng, T.; Zhang, X.; Mao, J.; Li, K.; Zhang, X. Synthesis of C_{60}-decorated SWCNTs (C_{60}-d-CNTs) and its TiO_2-based nanocomposite with enhanced photocatalytic activity for hydrogen production. *Dalton Trans.* **2013**, *42*, 3402−3409.
(46) Kumar, D.; Chen, M. S.; Goodman, D. W. Characterization of ultra-thin TiO_2 films grown on Mo(112). *Thin Solid Films.* **2006**, *515*, 1475−1479.
(47) Wang, X.; Yu, J. C.; Liu, P.; Wang, X.; Su, W.; Fu, X. Probing of photocatalytic surface sites on SO_4^{2-}/TiO_2 solid acids by in situ FTIR spectroscopy and pyridine adsorption. *J. Photochem. Photobiol., A* **2006**, *179*, 339−347.
(48) Parida, K. M.; Sahu, N.; Tripathi, A. K.; Kamble, V. S. Gold promoted S, N-doped TiO_2: An efficient catalyst for CO adsorption and oxidation. *Environ. Sci. Technol.* **2010**, *44*, 4155−4160.
(49) Hoffmann, M. R.; Martin, S. T.; Choi, W. Y.; Bahnemann, D. W. Environmental applications of semiconductor photocatalysis. *Chem. Rev.* **1995**, *95*, 69−96.
(50) Cao, J.; Xu, B.; Lin, H.; Luo, B.; Chen, S. Novel heterostructured Bi_2S_3/BiOI photocatalyst: Facile preparation, characterization and visible light photocatalytic performance. *Dalton Trans.* **2012**, *41*, 11482−11490.
(51) Jing, J.; Zhan, X.; Sun, P.; Zhang, L. ZnO/BiOI heterostructures: Photoinduced charge-transfer property and enhanced visible-light photocatalytic activity. *J. Phys. Chem. C* **2011**, *115*, 20555−20564.
(52) Zheng, L.; Zheng, Y.; Chen, C.; Zhan, Y.; Lin, X.; Zheng, Q.; Wei, K.; Zhu, J. Network structured SnO_2/ZnO heterojunction nanocatalyst with high photocatalytic activity. *Inorg. Chem.* **2009**, *48*, 1819−1825.
(53) Sasikala, R.; Shirole, A. R.; Sudarsan, V.; Kamble, V. S.; Sudakar, C.; Naik, R.; Rao, R.; Bharadwaj, S. R. Role of support on the photocatalytic activity of titanium oxide. *Appl. Catal., A* **2010**, *390*, 245−252.
(54) Pany, S.; Naik, B.; Martha, S.; Parida, K. M. Plasmon induced nano Au particle decorated over S, N-Modified TiO_2 for exceptional photocatalytic hydrogen evolution under visible light. *ACS Appl. Mater. Interfaces.* **2014**, *6*, 839−846.
(55) Sun, H.; Liu, H.; Ma, J.; Wang, X.; Wang, B.; Han, L. Preparation and characterization of sulfur-doped TiO_2/Ti photoelectrodes and their photoelectrocatalytic performance. *J. Hazard. Mater.* **2008**, *156*, 552−559.
(56) Parida, K. M.; Mohapatra, L.; Baliarsingh, N. Effect of Co^{2+} substitution in the framework of carbonate intercalated Cu/Cr LDH on structural, electronic, optical, and photocatalytic properties. *J. Phys. Chem. C* **2012**, *116*, 22417−22424.
(57) Ishibashi, K.; Fujishima, A.; Watanabe, T.; Hashimoto, K. Detection of active oxidative species in TiO_2 photocatalysis using the fluorescence technique. *Electrochem. Commun.* **2000**, *2*, 207−210.
(58) Roussel, H.; Briois, V.; Elkaim, E.; deRoy, A.; Besse, J. P. Cationic order and structure of [Zn-Cr-Cl] and [Cu-Cr-Cl] layered double hydroxides: A XRD and EXAFS study. *J. Phys. Chem. B* **2000**, *104*, 5915−5923.

DOI: 10.1021/sc500570k
ACS Sustainable Chem. Eng. 2015, 3, 245−253